



Universidad Autónoma
de Madrid

Biblos-e Archivo
Repositorio Institucional UAM

Repositorio Institucional de la Universidad Autónoma de Madrid

<https://repositorio.uam.es>

Esta es la **versión de autor** del artículo publicado en:
This is an **author produced version** of a paper published in:

Separation and Purification Technology 306.A (2023): 122570

DOI: <https://doi.org/10.1016/j.seppur.2022.122570>

Copyright: © 2022 Elsevier B.V. All rights reserved.

This manuscript version is made available under the CC-BY-NC-ND 4.0
licence <http://creativecommons.org/licenses/by-nc-nd/4.0/>

El acceso a la versión del editor puede requerir la suscripción del recurso
Access to the published version may require subscription

1 **A comprehensive study of the reduction of nitrate on natural FeTiO₃:**
2 **photocatalysis and DFT calculations**

3 Jefferson E. Silveira^{1,3}, Aramille S. de Souza², Fernando N. N. Pansini², Alyson R.
4 Ribeiro³, Wanderlã L. Scopel², Juan A. Zazo¹, Jose A. Casas¹ and Wendel S. Paz²

5 ¹Department of Chemical Engineering, Universidad Autónoma de Madrid, Cantoblanco, 28049 Madrid,
6 Spain

7 ²Department of Physics, Federal University of Espírito Santo, Vitória, ES 29075-910, Brazil ³Department
8 of Preventive Veterinary Medicine, Veterinary School, Federal University of Minas Gerais, ^{Minas}
9 Gerais, 31270-901, Brazil

10 Corresponding author: jefferson.silveira@uam.es wendel.paz@ufes.br

11

12 **ABSTRACT**

13 Experimental and theoretical investigation of the capacity of the natural ilmenite
14 (FeTiO₃) to reduce nitrate (NO₃⁻) from ultra-pure and mineral water is presented. A
15 comprehensive mechanism of NO₃⁻ photocatalytic transformation is proposed regarding
16 the density functional theory (DFT) calculations and the photocatalytic reduction of
17 nitrate. When ultra-pure water is employed, the nitrate is totally converted to NO_x (2%)
18 and N₂ (98%) after 210 minutes. Additionally, using the stoichiometric dose of oxalate,
19 the nitrate also vanishes from the mineral water, forming NO₂⁻, NO_x, and N₂ as
20 products. Thus, the findings reveal that natural ilmenite can be a great candidate for
21 reducing NO₃⁻ in contaminated water.

22

23

24

1. INTRODUCTION

Agricultural activities such as manure disposal in soil, chemical fertilization, and wastewater from intensive animal production have been indicated as major sources of nitrate contamination in water bodies, which can lead to negative effects on humans, animals, and the aquatic ecosystem. The control of nitrate (NO_3^-) concentration in the aquatic environment is important for several reasons, including the prevention of water acidification, the reduction of water eutrophication, and the reduction of toxicity to both human and aquatic organisms. Additionally, the intake of high concentrations of nitrate has been linked to methemoglobinemia [1], stomach cancer [2], "blue baby syndrome" or cyanosis [3] as well as a number of other still undetermined health consequences [4].

The World Health Organization suggests that NO_3^- concentration in drinking water should not exceed the acceptable limit of 50 mg L^{-1} [5]. Physical [6], chemical [7], and electrochemical processing techniques [8], as well as biological degradation and other treatment strategies [9] have been used to address aquatic NO_3^- contamination. However, those processes are related to mass transfer methodologies, incomplete nitrogen depletion, the formation of greenhouse gasses, and required post-treatments. Nevertheless, the treatment of nitrate-containing water and wastewater is still challenging, despite recent advancements [10]. The main unsolved difficulty is to develop a suitable catalyst capable of selectively reducing nitrates to nitrogen gas (N_2) while preventing the formation of additional dangerous nitrogenous byproducts, such as nitrite (NO_2^-) and ammonium (NH_4^+), that ultimately restrict water use for both human consumption and animal maintenance.

To overcome the limitations of conventional treatments, the catalytic and photocatalytic reduction of NO_3^- have been proposed [11]. In 1987 Akihiko Kudo

reported the first photocatalytic reduction of NO_3^- over Pd-TiO₂ [12]. From then onwards, many efforts were undertaken to photocatalytically reduce NO_3^- [13,14]. It is important to mention that N₂ selectivity is greatly reduced on pure TiO₂ because of an unexpectedly significant conversion into NO_2^- and NH_4^+ [15]. Additionally, the photogenerated holes and OH[•] radicals have the ability to oxidize the produced NO_2^- and NH_4^+ back to NO_3^- , which results in a photocatalytic reduction activity that is quite modest [16,17]. The reduction of NO_3^- can be accomplished in a time-efficient and cost-effective manner by the use of a photocatalyst that is technologically feasible.

Given these circumstances, the natural mineral ilmenite (FeTiO₃) has emerged as an interesting catalyst candidate for being safe, economical, and stable. This low-cost photocatalyst absorbs in the UV-Vis range due to its large band gap value, which depends on its polymorphism structure (ranging from 2.4 to 2.9 eV). Our research group recently revealed promising outcomes for the selective photo-reduction of nitrate to N₂ using FeTiO₃ and oxalic acid as reducing agents [18]. However, during natural water treatment, the presence of species in solution that compete with photogenerated holes and electrons over photocatalysts or redox mediators may dramatically influence effectiveness due to their adsorption onto the catalyst [19]. Therefore, monitoring the formation of active species involved in NO_x reduction is essential.

In order to develop more efficient photocatalysts, theoretical modeling, in particular Density Functional Theory (DFT), is a powerful tool to give a comprehensive understanding of the structural, electronic, and optical properties and also to reveal the reaction mechanisms that are difficult to explain by experimental techniques [20,21]. DFT calculations have been widely used to explore the properties of molecules adsorbate on materials surfaces, as well as the interaction of adsorbents on the adsorbate [22]. So far, several studies have analyzed the interactions between nitrogen oxide and

titanium oxide surfaces through DFT. Rodriguez et al. [23] studied the adsorption of nitrogen oxides (NO_2) on $\text{TiO}_2(110)$ single crystal, obtaining surface nitrate as the main product of the reaction by the disproportionation of NO_2 on Ti sites. Marutheeswaran et al. [24] investigated the electronic structure of NO_2 on the TiO_2 surface to predict and design its interaction in the presence of water vapor to generate gaseous nitrous acid.

In this report, a systematic investigation into the photocatalytic performance of catalyst FeTiO_3 samples was performed to obtain optimal efficiency. A comprehensive mechanism of NO_3^- photocatalytic transformation is provided based on theoretical simulations and identified products. Also, a practical approach was used to confirm the theoretical data.

2. MATERIAL AND METHODS

2.1. Reactants

All chemicals used were purchased from Sigma-Aldrich, USA. The ilmenite (Ref. 50110700) was provided by Marphil S.L. (Spain). The catalyst's main physical-chemical properties are gathered in [25]. The main parameters of the employed mineral water were: $\text{pH} = 7.7$, $\text{HCO}_3^- = 165 \text{ mg/L}$, $\text{SO}_4^{2-} = 3.7 \text{ mg/L}$, $\text{Cl}^- = 18.8$, $\text{Ca}^{2+} = 35.7$, $\text{Mg}^{2+} = 16.5 \text{ mg/L}$.

2.2. Theoretical Method

The quantum mechanical calculations were performed within the Density Functional Theory (DFT) framework, as implemented in the Quantum ESPRESSO package [26]. Based on the previous results obtained from Scanning Tunneling Microscopy (STM) and theoretical investigations of the (0001) ilmenite surface [25,27,28], a slab model has been proposed, where a (3 x 3) supercell of ilmenite

comprises 13 atomic layers separated by a vacuum region of 15 Å. The electron-ion interactions were described using the Projector Augmented Wave (PAW) method [29] and Perdew-Burke-Ernzerhof (PBE) Generalized Gradient Approximation (GGA) was used to approximate electronic exchange-correlation energy and the Grimme D3 correction to improve the description of the van der Waals interactions [30]. The energy cut-off for the plane-wave basis set is put at 65 Ry with a charge density cut-off of 650 Ry. A Monkhorst-Pack [31] scheme was used with a 5 x 5 x 3 (bulk) and 8 x 8 x 1 (slab) k-mesh for the Brillouin zone integration. When the geometry is optimized, the top three atomic layers and the molecules are allowed to relax, while the lower ten atomic layers are fixed. The atomic structure of FeTiO₃ was fully relaxed in the supercell approach based on the experimental lattice structure [32] and the geometry optimization was done with a convergence tolerance of 10⁻⁵ eV for the total energy and all the atoms were allowed to relax till the force was less than 10⁻³ Ry/a.u.

2.3. Typical practical reaction procedure

The experimental step was carried out in a cylindrical sealed glass jacketed batch reactor (useful volume: 750 mL; inner diameter: 0.15m), and operated under inert conditions through a continuous N₂ flow of 370 mL min⁻¹. As an inner radiation source, a commercial medium-pressure mercury lamp (150W) was used (TQ150 Heraeus, Germany). The lamp emits in a broad spectrum between 250 and 600 nm with a UV-irradiance of 30 W/m² measured with a broad range photoradiometer (Delta Ohm, model HD 2102.1). The lamp is placed inside a water refrigerated quartz tube (outer diameter 0.04 m). The system was maintained at 25 °C by recirculated water (Huber, Germany). A more detailed reaction procedure is described elsewhere [18-19].

The ilmenite load was previously set at 450 mg L⁻¹ [18-19] and used the stoichiometric dose of oxalate (0.18 g L⁻¹) needed for the complete reduction of NO₃⁻ (50 mg L⁻¹) to N₂. All experiments have been performed in triplicate and lasted 210 minutes, using deionized water and mineral water without pH modification as solvents. Samples were collected, filtered through 0.45 µm, and then promptly examined at predetermined intervals.

2.4. Analytical methodology

The quantification of nitrate, nitrite, and oxalic acid was performed using ion chromatography (IC) with chemical suppression (Metrohm 790 IC) coupled to a conductivity detector [25]. NO_x concentrations in the gas phase were assessed using a chemiluminescence NO_x analyzer (CLD 63 Ecophysics) and recorded in 1 second intervals. Total nitrogen (TN) were measured with a TNM analyzer (Shimadzu). The difference between the initial TN and the sum of the N in the compounds (NO₃⁻, NO₂⁻, NO_x) is attributed to the formation of N₂.

3. RESULTS AND DISCUSSION

3.1. Electronic structure calculations

Pristine ilmenite (FeTiO₃) has a rhombohedral crystal structure in space group $R\bar{3}$ with the hexagonal packing of the oxygen atoms with cations occupying two-thirds of the octahedral positions, where Fe and Ti occupy alternating layers. Periodic boundary conditions were applied with a vacuum of 15 Å in the z-axis to prevent interactions between the system and its periodic image. The complete hexagonal unit cell of ilmenite is presented in Figure 1(a). The experimental FeTiO₃ lattice structure was obtained from the American Mineralogist Crystal Structure Database [32], and the

super-cell method was used to fully relax the atomic structure. The calculated lattice parameters for FeTiO_3 are $a = b = 5.143 \text{ \AA}$ and $c = 13.98 \text{ \AA}$, which are quite close with the experiment data, in which $a = b = 5.087 \text{ \AA}$ and $c = 14.013 \text{ \AA}$ [32]. Based on the optimized structures, a simulated X-ray diffraction (XRD) spectrum of pristine ilmenite was made using the VESTA Crystallographic Software as shown in Figure S1. The peaks in the simulated DFT spectrum (no refinement) match very closely with experimental XRD measurement.

To obtain insight into the electronic properties of the FeTiO_3 bulk, its band structure was obtained by first-principle calculations based on the crystal structure given above, resulting in an indirect bandgap of 1.68 eV. Overestimation of electron delocalization in systems with d-localized electrons is a known shortcoming in the DFT approach owing to unphysical self-interaction. In order to get more trustworthy values, maybe closer to those obtained experimentally, the DFT+U approach was considered, which involves explicitly treating electronic correlation using a Hubbard-like model for a subset of states in the system [33]. By using the DFT+U approach, an indirect bandgap of 2.6 eV was obtained, which can be seen in Figure 1b, consistent with ilmenite values reported in the literature (between 2.5 and 2.9 eV) [34, 35].

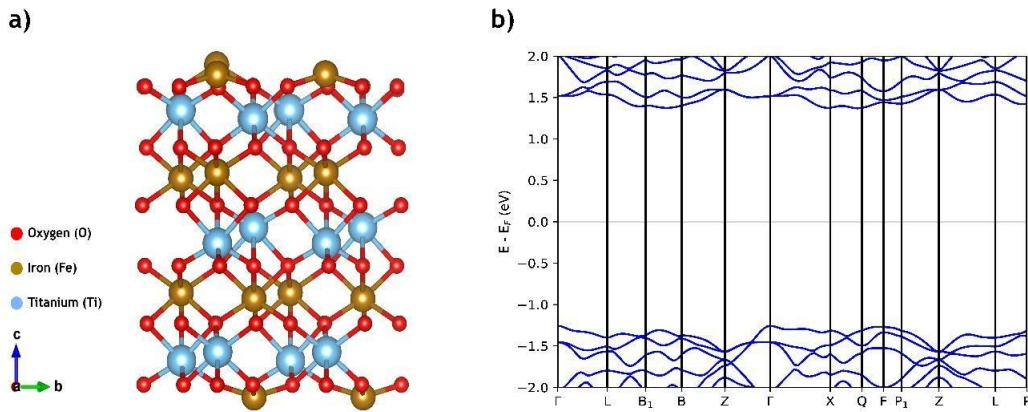


Fig. 1 (a) Crystal structure of FeTiO_3 ilmenite and (b) DFT+U band structure calculation of bulk FeTiO_3 .

When light is incident on a semiconductor, photons can produce pairs of electrons/holes. The excited electrons can then participate in the hydrogen reduction process (HER) in an aqueous environment, producing H_2 : $2H^+ + 2e^- \rightarrow H_2$. The holes, on the other hand, take part in the oxidation reaction (OER) that produces O_2 : $H_2O + 2h^+ \rightarrow 1/2 O_2 + 2H^+$. The appropriate photocatalyst material for HER must have a Conduction Band Minimum (CBM) energy greater than the reduction potential of H^+/H_2 and a Valence Band Maximum (VBM) energy less than the oxidation potential of O_2/H_2O . In this context, different $FeTiO_3$ surface terminations were considered and for the most stable one with O-termination (see Figure 2b), it was verified that the CBM alignment is 50 meV, lower than the free energy of water reduction (SHE), whereas for the ilmenite bulk phase it was 0.1 eV [36].

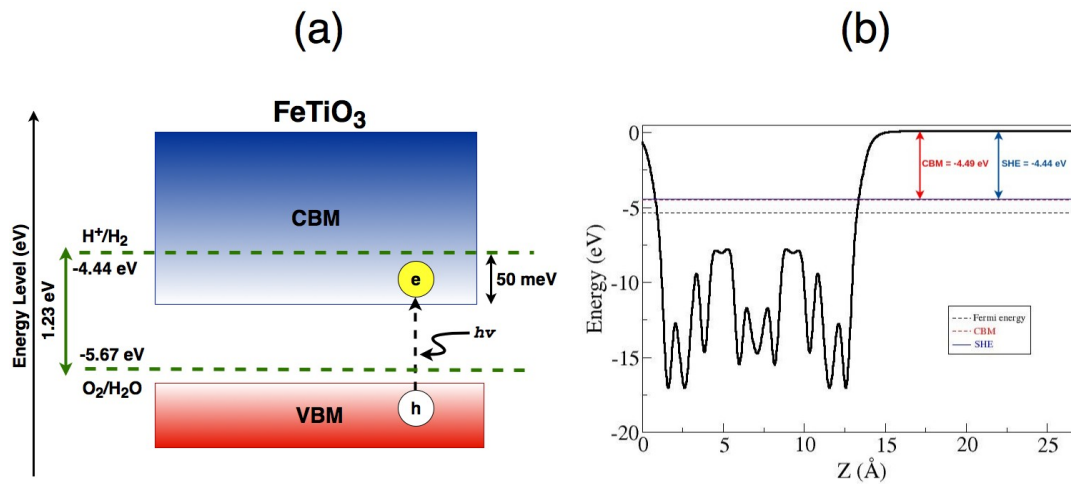


Fig. 2. (a) Band edge positions of $FeTiO_3$ relative to the vacuum level with GGA-PBE functional. The standard redox potentials for water splitting at $pH = 0$ are shown for comparison aligned with reference to the redox potentials for water splitting (b) Electrostatic potential of the slab Ilmenite ($\sim 12.0 \text{ \AA}$) along the z-direction.

The HER and OER potentials for water change with pH as $(-4.44 + \text{pH} \times 0.059 \text{ eV})$ and $(-5.67 + \text{pH} \times 0.059 \text{ eV})$, respectively, which shift the water's redox energy levels in Figure 2a upward [37]. So, this change is favorable to OER reduction for FeTiO₃ because the oxidation energy level at pH = 0 is lower than the oxidation potential for O₂/H₂O. On the other hand, higher pH values lead to the reduction processes being less energetically beneficial. Thus, FeTiO₃ is a suitable photocatalyst for O₂ evolution in the presence of an electron acceptor such as K⁺, Ca²⁺, Mg²⁺, and Fe³⁺ under visible light irradiation, but it is not active for H₂ (H⁺ generation) evolution due to its low conduction band level.

3.1.1 Molecules on FeTiO₃ surface

In order to better understand the mechanisms of NO₃⁻ reduction reactions, the binding energies of C₂O₄²⁻ and NO₂⁻ on the O-terminated FeTiO₃ surface were also investigated, once the adsorption of the reactants is the first step in this heterogeneous reaction. Some possible adsorption configurations were examined in order to establish which configurations were the most promising for each adsorbate. To do this, the adsorption energy was calculated by

$$E_b = \left[E_{\left(\begin{smallmatrix} \text{slab} \\ \text{mol} \end{smallmatrix} \right)} - (E_{\text{slab}} + E_{\text{mol}}) \right] \quad (\text{Eq. 1})$$

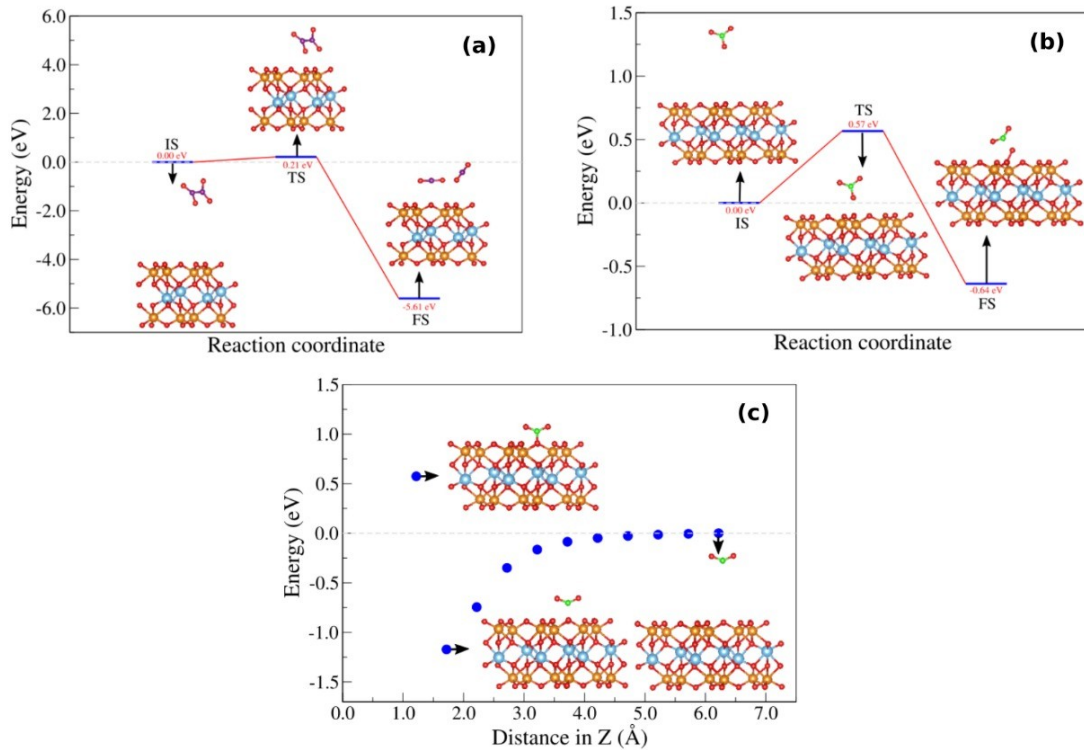
where the binding energy (E_b) is defined as follows: E_{mol} is the energy of an isolated molecule; E_{slab} is the energy of clean (0 0 1) FeTiO₃ surface slab, and $E_{\text{slab/mol}}$ is the total energy of the surface with adsorbed molecules. According to Eq (1), $E_b < 0$ indicates an exothermic process. The charge difference density is a measure of how much charge is transferred between different regions. The expression (Eq. 2) is as follows:

213

$$214 \quad \Delta\rho(r) = \rho_{\text{molecule/slab}}(r) - \rho_{\text{slab}}(r) - \rho_{\text{molecule}}(r) \text{ (Eq. 2)}$$

215 where, $\rho_{\text{molecule/slab}}$, ρ_{slab} , and ρ_{molecule} represent the total charge density of the system after
 216 adsorption, the charge density of the substrate before adsorption, and the charge density
 217 of free gas molecules, respectively. Bader charge population analysis is used to
 218 investigate charge transfer on the surface before and after gas adsorption [38]. A
 219 negative number indicates an electron gain, while a positive number represents an
 220 electron loss. The adsorption formation energy, charge transfer, and minor distance
 221 between molecule and surface for the most energetic stable configurations for each
 222 molecule adsorbate on an O-terminated surface are presented in Table I.

223



224 **Fig. 3.** Initial structure (IS), transition structure (TS), and final structure (FS)
 225 calculations for the (a) $\text{C}_2\text{O}_4^{2-}$, (b) NO_3^- , and schematic energy profile for the NO_2^-
 226 reduction (c) on the O-terminated FeTiO_3 surface.

Table I. Energetic properties of the adsorbed systems. Geometrical parameters (distances), binding energies (eV/supercell), and Bader charge (e) of the adsorbed gasses $\text{C}_2\text{O}_4^{2-}$, NO_3^- , and NO_2^- on the FeTiO_3 surface.

Molecule	$d_{\text{C-Fe}}$ (Å)	$d_{\text{N-Fe}}$ (Å)	$d_{\text{O-Fe}}$ (Å)	E_b (eV)/supercell	q (e)
$\text{C}_2\text{O}_4^{2-}$	3.02	-	1.90	- 1.43	0.17
NO_2^-	-	1.78	2.06	- 2.35	0.65
NO_3^-	-	2.39	1.96	- 3.34	0.68

According to the findings of the Bader charge analysis (Table I), there is a transfer of 0.17, 0.65, and 0.68 e from the FeTiO_3 surface to the $\text{C}_2\text{O}_4^{2-}$, NO_2^- , and NO_3^- , respectively. For the NO_2^- and NO_3^- molecules, one can observe that the highest charge transfer is related to the highest binding energy, and the distance between the surface and the O atom of the molecule is around 2 Å, which indicates the formation of chemical bonds between the O atoms and the FeTiO_3 surface. In the case of $\text{C}_2\text{O}_4^{2-}$, due to its interaction with surface, it was noted that molecule is split into two CO_2 molecules with 0.17 e transferred from surface to $\text{C}_2\text{O}_4^{2-}$.

In a noncatalytic gas-phase environment and with the more stable configurations of each molecule adsorbed on the surface, it was performed reaction coordinate calculations with Initial Structures (IS), Transition Structure (TS), and Final Structure (FS) for the NO_3^- , NO_2^- , and $\text{C}_2\text{O}_4^{2-}$ to get their reaction barriers, as shown in Figure 3. The employed calculation model consists of a (3 x 3) supercell of ilmenite with a surface terminated by a Fe/O atom and molecules of NO_3^- , NO_2^- , and $\text{C}_2\text{O}_4^{2-}$ positioned close to the surface. The initial and final states, which both match the ideal adsorption geometries previously found, were considered in order to estimate the energy barrier. As shown in Figure 3a, the energy required to split an adsorbed $\text{C}_2\text{O}_4^{2-}$ molecule is only 0.21 eV/supercell, implying that cracking into two CO_2 molecules under UV-Vis is

rather simple, supporting the experimental findings, in which a high concentration of (CO₂) was detected, when irradiating UV-Vis in a system containing FeTiO₃ and oxalic acid. The role of the reducing agent in N₂ selectivity will be better discussed below. Figures 3b and 3c, illustrate that, following the supercell relaxations, both NO₃⁻ and NO₂⁻ molecules are adsorbed by an O surface atom on the pristine FeTiO₃, and the energy barrier for NO₃⁻ is ~ 0.55 eV, whereas there is no energy barrier for NO₂⁻ adsorption. The minor distance between NO₃⁻ and Fe atoms is approximately 1.94 Å and between NO₂⁻ and Fe atoms is approximately 1.78 Å, as shown in Table I.

3.1.2 Experimental approach

Experiments using two aqueous matrices (ultrapure water and mineral water) were carried out to validate the theoretical outcomes (Figure 4).

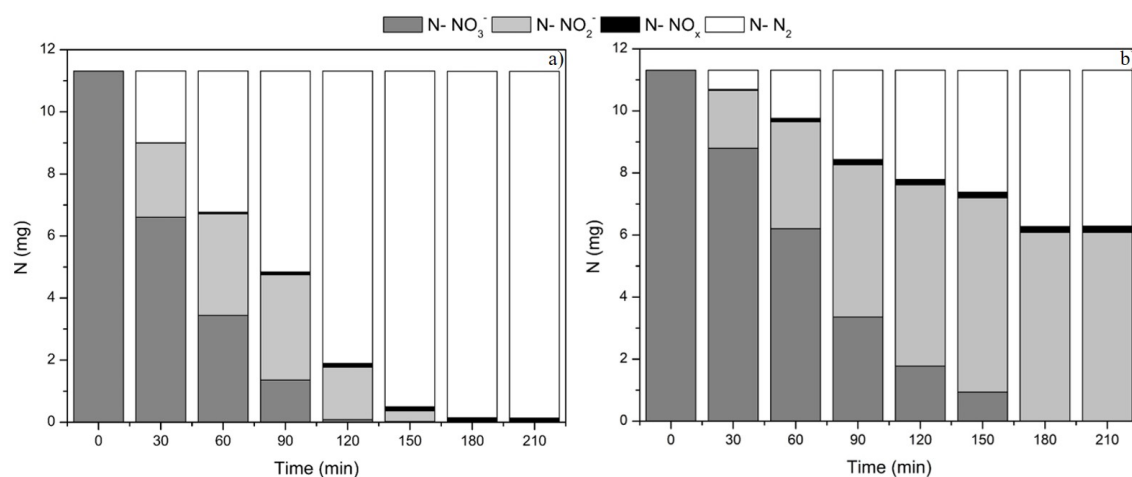
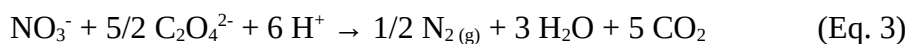


Fig. 4. Effect of water matrix on the photocatalytic reduction of NO₃⁻: Experimental conditions: ultrapure water (a) mineral water (b). [FeTiO₃]₀= 450 mg L⁻¹, [C₂O₄²⁻]₀ = 0.18 g L⁻¹, [NO₃⁻] = 50 mg L⁻¹

As can be observed in Figure 4a, in the presence of oxalate, NO₃⁻ concentration reduces to NO₂⁻. Afterwards, nitrite is completely converted to NO_x and N₂ (Eq. 3).



A selectivity to N_2 higher than 98% was obtained following 210 minutes of reaction. At the same time, NO_x in the control experiment does not reach 2% (Figure 4a). Using the stoichiometric dose of $\text{C}_2\text{O}_4^{2-}$ needed to complete nitrogen elimination in mineral water, it was observed a sharp decrease in the NO_3^- reduction, leading to an intense impairment in the process efficiency (Figure 4b). Figure 5 depicts the excess of hole scavengers effect on the nitrate reduction during the 210 min of reaction in different experimental conditions. It is interesting to note that when a dose of $\text{C}_2\text{O}_4^{2-}$ equal to 150 % of the stoichiometric amount required for the reduction of nitrate was used, N_2 selectivity values of 95 % were achieved for mineral water.

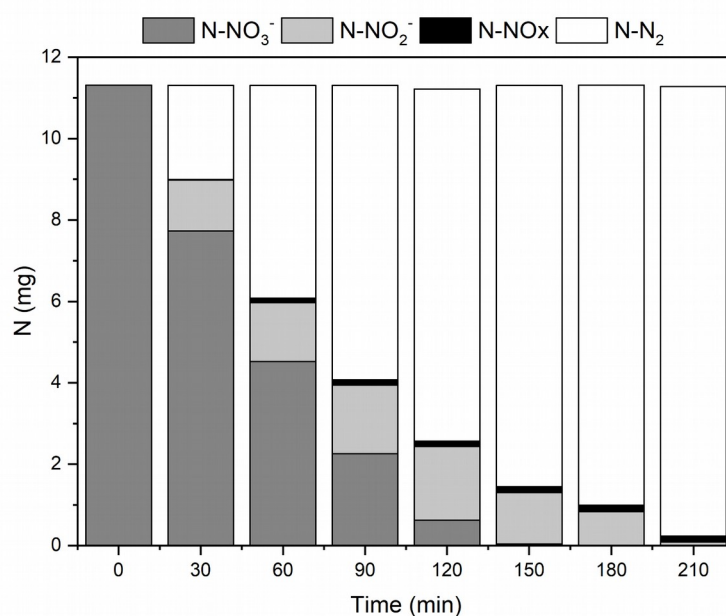
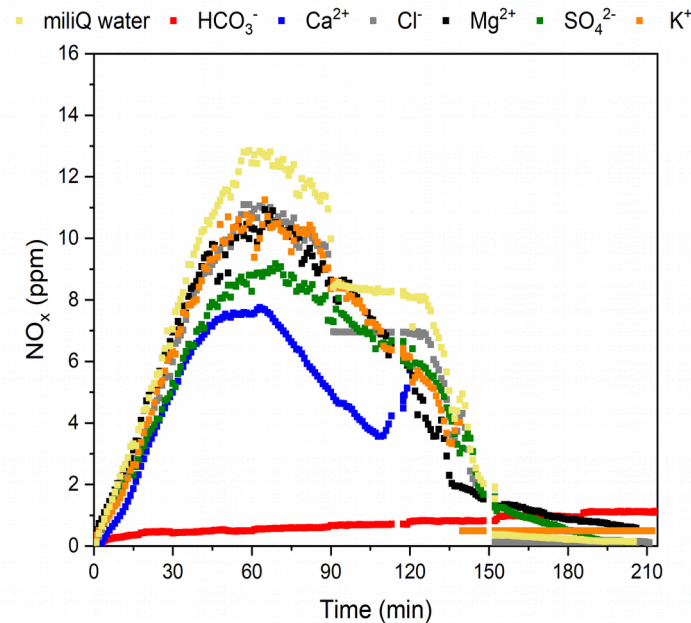


Fig. 5. Experiments using an excess of hole scavengers. Time evolution of NO_3^- photo-reduction. Experimental conditions: $[\text{FeTiO}_3] = 450 \text{ mg/L}$, $[\text{NO}_3^-] = 50 \text{ mg L}^{-1}$, $[\text{C}_2\text{O}_4^{2-}] = 150\%$, $T = 25^\circ\text{C}$.

284 In a previous work [39] the lower NO_3^- conversion was linked with the presence
 285 of ions in the aqueous matrix, mainly HCO_3^- and Ca^{2+} . In an attempt to get closer to the
 286 experimental observations, it was investigated the role of HCO_3^- on the surface and its
 287 implications on the barrier energy of NO_3^- and NO_2^- at the FeTiO_3 surface. In the case of
 288 Ca^{2+} , its role is related to CaC_2O_4 precipitation. On the other hand, the findings indicate
 289 that HCO_3^- has the largest effect on the energy barrier for NO_3^- and (NO_2^-) adsorptions,
 290 where the barrier increases from 0.57 (no barrier) eV/supercell on the clean surface to
 291 2.66 (2.07) eV/supercell on the high HCO_3^- coverage surface, respectively, as shown in
 292 Figure (S2). The energy barrier in theoretical calculations corresponds to the
 293 experimental activation energy, which represents the height of the barrier. The
 294 activation energy can serve as an indicator of the difficulty of a chemical reaction.
 295 These larger activation energy barriers are consistent with the experimental findings
 296 that, as deduced from Figure 6, bicarbonate induced a greater decrease in NO_x
 297 production and, as a result, the selectivity toward N_2 dropped below 40 %.



298
 299 Fig. 6. Effect of isolated ions: generation of NO_x . Experimental conditions: $[\text{FeTiO}_3]_0 =$
 300 450 mg L^{-1} , $[\text{C}_2\text{O}_4^{2-}]_0 = 100\%$, $[\text{NO}_3^-] = 50 \text{ mg L}^{-1}$.

4. CONCLUSION

This study provides the mechanisms of the NO_3^- reduction reaction on FeTiO_3 , as well as the influence of the operating conditions on the efficiency of NO_3^- removal. Supporting the obtained experimental data, which finds a high concentration of CO_2 in the presence of UV-Vis light, the DFT simulations show that the energy required to split an adsorbed oxalate is only 0.21 eV/supercell. The presented ab initio calculations also indicate that the interaction of the NO_3^- and NO_2^- with the FeTiO_3 surface is responsible for reducing the NO_3^- molecule. These theoretical results agree with the experimental data for ultrapure and mineral water. In the case of ultrapure water combined with oxalate, the NO_3^- molecule reduces to NO_2^- and later, the nitrite is converted to NO_x and N_2 . Thus, FeTiO_3 can be a great material to reduce the NO_3^- concentration present in the water, and the photocatalytic treatment that was performed in this work seems to be a viable alternative.

Acknowledgements

This work has been supported by MINECO through the project PID2019-106884GB-I00. Jefferson E. Silveira gratefully acknowledged the support Science Without Borders Program, Ministry of Education Brazil, under grant BEX-1046/13-6. The authors acknowledge financial support from Brazilian government funding agencies FAPES, CAPES and CNPq. Wendel S. Paz would also like to thank FAPES (under grant 444/2021) and CNPq (under grant 409441/2021-0) for their financial support.

325 REFERENCES

- 326 [1] Fan, A. M., Willhite, C. C., & Book, S. A. (1987). Evaluation of the nitrate
 327 drinking water standard with reference to infant methemoglobinemia and
 328 potential reproductive toxicity. *Regulatory Toxicology and pharmacology*, 7(2),
 329 135-148. [https://doi.org/10.1016/0273-2300\(87\)90024-9](https://doi.org/10.1016/0273-2300(87)90024-9).
- 330 [2] Karagas, M. R., Choi, A. L., Oken, E., Horvat, M., Schoeny, R., Kamai, E., ... &
 331 Korrick, S. (2012). Evidence on the human health effects of low-level
 332 methylmercury exposure. *Environmental health perspectives*, 120(6), 799-806.
 333 <https://doi.org/10.1289/ehp.1104494>
- 334 [3] Ihnken, K., Morita, K., Buckberg, G. D., Winkelmann, B., Schmitt, M., Ignarro,
 335 L. J., ... & Ihnken, K. (1997). Nitric-oxide-induced reoxygenation injury in the
 336 cyanotic immature heart is prevented by controlling oxygen content during initial
 337 reoxygenation. *Angiology*, 48(3), 189-202.
 338 <https://doi.org/10.1177/000331979704800301>.
- 339 [4] Fewtrell, L. (2004). Drinking-water nitrate, methemoglobinemia, and global
 340 burden of disease: a discussion. *Environmental health perspectives*, 112(14),
 341 1371-1374. <https://doi.org/10.1289/ehp.7216>.
- 342 [5] Herschy, R.W., Water Quality for Drinking: WHO Guidelines. In: Bengtsson, L.,
 343 Herschy, R.W., Fairbridge, R.W. (Eds.) *Encyclopedia of Lakes and Reservoirs*.
 344 *Encyclopedia of Earth Sciences Series*. Springer, Dordrecht, 2012, pp. 876–883.
 345 https://doi.org/10.1007/978-1-4020-4410-6_184.
- 346 [6] Bhatnagar, A., & Sillanpää, M. (2011). A review of emerging adsorbents for
 347 nitrate removal from water. *Chemical Engineering Journal*, 168(2), 493-504.
 348 <https://doi.org/10.1016/j.cej.2011.01.103>.
- 349 [7] Barrabés, N., & Sá, J. (2011). Catalytic nitrate removal from water, past, present

350 and future perspectives. *Applied Catalysis B: Environmental*, 104(1-2), 1-5.
 351 <https://doi.org/10.1016/j.apcatb.2011.03.011>.

352 [8] Peel, J. W., Reddy, K. J., Sullivan, B. P., & Bowen, J. M. (2003). Electrocatalytic
 353 reduction of nitrate in water. *Water Research*, 37(10), 2512-2519. [https://doi.org/](https://doi.org/10.1016/S0043-1354(03)00008-3)
 354 [10.1016/S0043-1354\(03\)00008-3](https://doi.org/10.1016/S0043-1354(03)00008-3).

355 [9] Kapoor, A., & Viraraghavan, T. (1997). Nitrate removal from drinking water.
 356 *Journal of environmental engineering*, 123(4), 371-380.
 357 [https://doi.org/10.1061/\(asce\)0733-9372\(1997\)123:4\(371\)](https://doi.org/10.1061/(asce)0733-9372(1997)123:4(371)).

358 [10] Hérissan, A., Meichtry, J. M., Remita, H., Colbeau-Justin, C., & Litter, M. I.
 359 (2017). Reduction of nitrate by heterogeneous photocatalysis over pure and
 360 radiolytically modified TiO₂ samples in the presence of formic acid. *Catalysis*
 361 *Today*, 281, 101-108. <https://doi.org/10.1016/j.cattod.2016.05.044>.

362 [11] Tugaoen, H. O. N., Garcia-Segura, S., Hristovski, K., & Westerhoff, P. (2017).
 363 Challenges in photocatalytic reduction of nitrate as a water treatment technology.
 364 *Science of the total environment*, 599, 1524-1551.
 365 <https://doi.org/10.1016/j.scitotenv.2017.04.238>.

366 [12] Kudo, A., Domen, K., Maruya, K. I., & Onishi, T. (1987). Photocatalytic
 367 reduction of NO₃⁻ to form NH₃ over Pt-TiO₂. *Chemistry Letters*, 16(6), 1019-
 368 1022. <https://doi.org/10.1246/cl.1987.1019>.

369 [13] Yue, M., Wang, R., Cheng, N., Cong, R., Gao, W., & Yang, T. (2016). ZnCr₂S₄:
 370 Highly effective photocatalyst converting nitrate into N₂ without over-reduction
 371 under both UV and pure visible light. *Scientific reports*, 6(1), 1-11.
 372 <https://doi.org/10.1038/srep30992>.

373 [14] Wang, R., Yue, M., Cong, R., Gao, W., & Yang, T. (2015). Photocatalytic
 374 reduction of nitrate over chalcopyrite CuFe_{0.7}Cr_{0.3}S₂ with high N₂ selectivity.

375 *Journal of Alloys and Compounds*, 651, 731-736.
 376 <https://doi.org/10.1016/j.jallcom.2015.08.182>.

377 [15] Hirakawa, H., Hashimoto, M., Shiraishi, Y., & Hirai, T. (2017). Selective nitrate-
 378 to-ammonia transformation on surface defects of titanium dioxide photocatalysts.
 379 *ACS Catalysis*, 7(5), 3713-3720. <https://doi.org/10.1021/acscatal.7b00611>.

380 [16] Zuo, X., Hu, J., & Chen, M. (2015). The role and fate of inorganic nitrogen
 381 species during UVA/TiO₂ disinfection. *Water Research*, 80, 12-19.
 382 <https://doi.org/10.1016/j.watres.2015.05.018>.

383 [17] Zhao, X., Zhang, G., & Zhang, Z. (2020). TiO₂-based catalysts for photocatalytic
 384 reduction of aqueous oxyanions: State-of-the-art and future prospects.
 385 *Environment international*, 136, 105453.
 386 <https://doi.org/10.1016/j.envint.2019.105453>.

387 [18] Zazo, J. A., García-Muñoz, P., Pliego, G., Silveira, J. E., Jaffe, P., & Casas, J. A.
 388 (2020). Selective reduction of nitrate to N₂ using ilmenite as a low cost photo-
 389 catalyst. *Applied Catalysis B: Environmental*, 273, 118930.
 390 <https://doi.org/10.1016/j.apcatb.2020.118930>.

391 [19] Silveira, J. E., Ribeiro, A. R., Carbajo, J., Pliego, G., Zazo, J. A., & Casas, J. A.
 392 (2021). The photocatalytic reduction of NO₃⁻ to N₂ with ilmenite (FeTiO₃):
 393 Effects of groundwater matrix. *Water Research*, 200, 117250.
 394 <https://doi.org/10.1016/j.watres.2021.117250>.

395 [20] Pérez-Casany, M. P., Nebot-Gil, I., & Sánchez-Marín, J. (2000). DFT theoretical
 396 study on the reaction mechanism of the nitrate radical with alkenes: 2-Butene,
 397 isobutene, 2-methyl-2-butene, and 2, 3-dimethyl-2-butene. *The Journal of*
 398 *Physical Chemistry A*, 104(46), 10721-10730. <https://doi.org/10.1021/jp000666f>

399 [21] Jones, R. O. (2015). Density functional theory: Its origins, rise to prominence,

400 and future. *Reviews of modern physics*, 87(3), 897.
 401 <https://doi.org/10.1103/RevModPhys.87.897>.

402 [22] Cohen, A. J., Mori-Sánchez, P., & Yang, W. (2012). Challenges for density
 403 functional theory. *Chemical reviews*, 112(1), 289-320.
 404 <https://doi.org/10.1021/cr200107z>

405 [23] Rodriguez, J. A., Jirsak, T., Liu, G., Hrbek, J., Dvorak, J., & Maiti, A. (2001).
 406 Chemistry of NO₂ on oxide surfaces: formation of NO₃ on TiO₂ (110) and
 407 NO₂ ↔ O vacancy interactions. *Journal of the American Chemical Society*,
 408 123(39), 9597-9605. <https://doi.org/10.1021/ja011131i>

409 [24] Marutheeswaran, S., Mishra, S. B., Roy, S. C., & Nanda, B. R. K. (2020).
 410 Mechanistic understanding of NO₂ dissociation on a rutile TiO₂ (110) surface:
 411 an electronic structure study. *The Journal of Physical Chemistry C*, 124(16),
 412 8786-8794. <https://doi.org/10.1021/acs.jpcc.0c00525>.

413 [25] Silveira, J. E., Paz, W. S., Garcia-Munoz, P., Zazo, J. A., & Casas, J. A. (2017).
 414 UV-LED/ilmenite/persulfate for azo dye mineralization: The role of sulfate in the
 415 catalyst deactivation. *Applied Catalysis B: Environmental*, 219, 314-321. <https://doi.org/10.1016/j.apcatb.2017.07.072>.

417 [26] Giannozzi, P., Baroni, S., Bonini, N., Calandra, M., Car, R., Cavazzoni, C., ... &
 418 Wentzcovitch, R. M. (2009). QUANTUM ESPRESSO: a modular and open-
 419 source software project for quantum simulations of materials. *Journal of physics:*
 420 *Condensed matter*, 21(39), 395502. [https://doi.org/10.1088/0953-](https://doi.org/10.1088/0953-8984/21/39/395502)
 421 [8984/21/39/395502](https://doi.org/10.1088/0953-8984/21/39/395502).

422 [27] Puthirath Balan, A., Radhakrishnan, S., Kumar, R., Neupane, R., Sinha, S. K.,
 423 Deng, L., ... & Ajayan, P. M. (2018). A non-van der Waals two-dimensional
 424 material from natural titanium mineral ore ilmenite. *Chemistry of Materials*,

425 30(17), 5923-5931. <https://doi.org/10.1021/acs.chemmater.8b01935>.

426 [28] Fellows, R. A., Lennie, A. R., Munz, A. W., Vaughan, D. J., & Thornton, G.
427 (1999). Structures of FeTiO₃ (0001) surfaces observed by scanning tunneling
428 microscopy. *American Mineralogist*, 84(9), 1384-1391.
429 <https://doi.org/10.2138/am-1999-0916>

430 [29] Pickard, C. J., & Mauri, F. (2001). All-electron magnetic response with
431 pseudopotentials: NMR chemical shifts. *Physical Review B*, 63(24), 245101.
432 <https://doi.org/10.1103/PhysRevB.63.245101>.

433 [30] Perdew, J. P., Burke, K., & Ernzerhof, M. (1996). Generalized gradient
434 approximation made simple. *Physical review letters*, 77(18), 3865.
435 <https://doi.org/10.1103/PhysRevLett.77.3865>.

436 [31] Pack, J. D., & Monkhorst, H. J. (1977). " Special points for Brillouin-zone
437 integrations"—a reply. *Physical Review B*, 16(4), 1748.
438 <https://doi.org/10.1103/PhysRevB.16.1748>.

439 [32] Wechsler, B. A., & Prewitt, C. T. (1984). Crystal structure of ilmenite (FeTiO₃)
440 at high temperature and at high pressure. *American Mineralogist*, 69(1-2), 176-
441 185. [https://pubs.geoscienceworld.org/msa/ammin/article-pdf/69/1-](https://pubs.geoscienceworld.org/msa/ammin/article-pdf/69/1-2/176/4216798/am69_176.pdf)
442 [2/176/4216798/am69_176.pdf](https://pubs.geoscienceworld.org/msa/ammin/article-pdf/69/1-2/176/4216798/am69_176.pdf)

443 [33] Liechtenstein, A. I., Anisimov, V. I., & Zaanen, J. (1995). Density-functional
444 theory and strong interactions: Orbital ordering in Mott-Hubbard insulators.
445 *Physical Review B*, 52(8), R5467. <https://doi.org/10.1103/PhysRevB.52.R5467>

446 [34] Raghavender, A. T., Hong, N. H., Lee, K. J., Jung, M. H., Skoko, Z.,
447 Vasilevskiy, M., ... & Samantilleke, A. P. (2013). Nano-ilmenite FeTiO₃:
448 Synthesis and characterization. *Journal of magnetism and magnetic materials*,
449 331, 129-132. <https://doi.org/10.1016/j.jmmm.2012.11.028>.

- [35] Charilaou, M., Sheptyakov, D., Löffler, J. F., & Gehring, A. U. (2012). Large spontaneous magnetostriction in FeTiO₃ and adjustable magnetic configuration in Fe (III)-doped FeTiO₃. *Physical Review B*, 86(2), 024439. <https://doi.org/10.1103/PhysRevB.86.024439>.
- [36] Gao, B., Kim, Y. J., Chakraborty, A. K., & Lee, W. I. (2008). Efficient decomposition of organic compounds with FeTiO₃/TiO₂ heterojunction under visible light irradiation. *Applied Catalysis B: Environmental*, 83(3-4), 202-207. <https://doi.org/10.1016/j.apcatb.2008.02.017>.
- [37] Chakrapani, V., Angus, J. C., Anderson, A. B., Wolter, S. D., Stoner, B. R., & Sumanasekera, G. U. (2007). Charge transfer equilibria between diamond and an aqueous oxygen electrochemical redox couple. *science*, 318(5855), 1424-1430. <https://doi.org/10.1126/science.1148841>.
- [38] Bader, R. F. (1985). Atoms in molecules. *Accounts of Chemical Research*, 18(1), 9-15. <https://doi.org/10.1021/ar00109a003>.
- [39] Silveira, J. E., Ribeiro, A. R., Carbajo, J., Pliego, G., Zazo, J. A., & Casas, J. A. (2021). The photocatalytic reduction of NO₃⁻ to N₂ with ilmenite (FeTiO₃): Effects of groundwater matrix. *Water Research*, 200, 117250. <https://doi.org/10.1016/j.watres.2021.117250>.

**A comprehensive study of the reduction of nitrate on natural FeTiO₃:
photocatalysis and DFT calculations**

Jefferson E. Silveira^{1,3}, Aramille S. de Souza², Fernando N. N. Pansini², Alyson R.
Ribeiro³, Wanderlã L. Scopel², Juan A. Zazo¹, Jose A. Casas¹ and Wendel S. Paz²

¹Department of Chemical Engineering, Universidad Autónoma de Madrid, Cantoblanco, 28049 Madrid,
Spain

²Departamento de Física, Universidade Federal do Espírito Santo, Vitória, ES 29075-910, Brazil

³Department of Preventive Veterinary Medicine, Veterinary School, Federal University of Minas Gerais,
Minas Gerais, 31270-901, Brazil

Corresponding author: jefferson.silveira@uam.es, wendel.paz@ufes.br

Supplementary Information

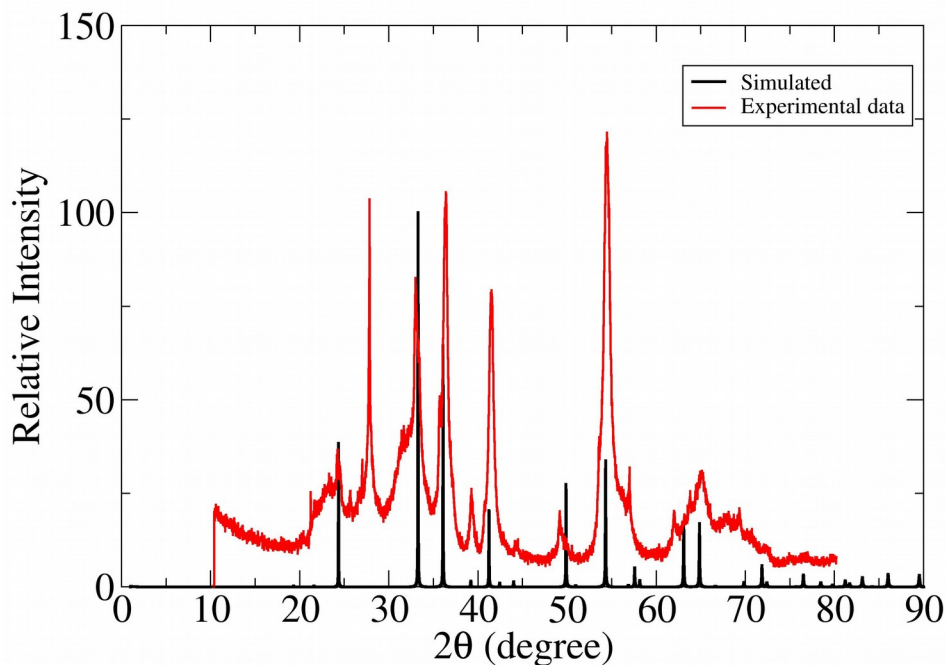
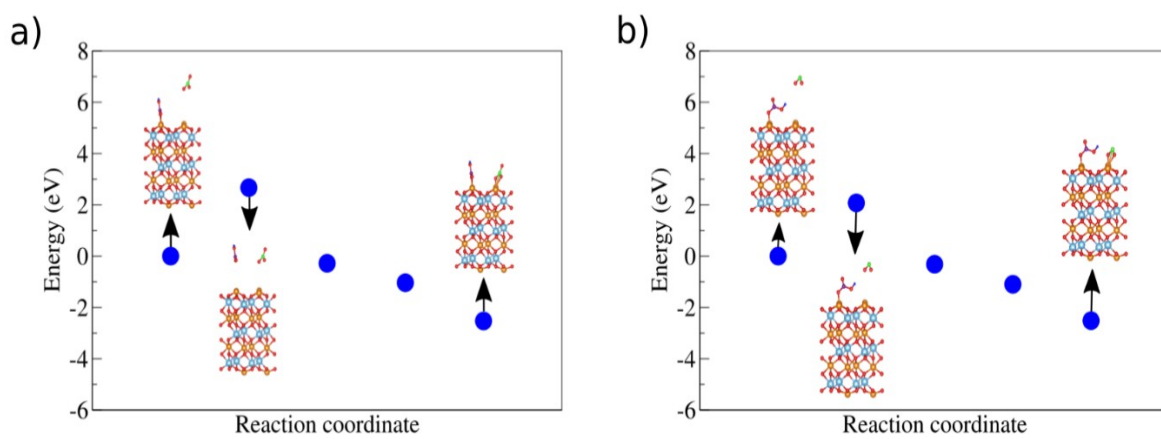


Fig. S1. Experimental and simulated XRD patterns of pristine ilmenite.

487



488

489 **Fig. S2.** Schematic energy profile for the HCO_3^- on O-terminated FeTiO_3 surface.

490

491